ELSEVIER

Ceramics International 33 (2007) 543–550

CERAMICS INTERNATIONAL

www.elsevier.com/locate/ceramint

Mechanical behaviour and thermal and electrical properties of foam glass

François Méar *, Pascal Yot, Romain Viennois, Michel Ribes

Equipe de Recherche Technologique 3 "Caractérisation des Matériaux", Laboratoire de Physicochimie de la Matière Condensée, UMR CNRS 5617, Université Montpellier II, CC 003, Place Eugène Bataillon, 34095 Montpellier, Cedex 5, France

Received 19 September 2005; received in revised form 10 October 2005; accepted 14 November 2005
Available online 7 February 2006

Abstract

Cellular glasses were synthesised by heat treatment (750–850 °C for 60–120 min) of waste cathode-ray tube (CRT) glasses (funnel and panel) with a SiC or TiN reducing agent. Macro-size pores with a single distribution were formed after reduction with SiC, whereas a double distribution was observed for TiN. The intrinsic properties of these materials were investigated. We found that the flexural strengths of the samples varied from 4 to 68 MPa depending on their porosity, and that the compressive strengths varied from 4 to 267 MPa. Our analysis shows that Ashby's model is more appropriate for these porous materials because their Poisson ratios are porosity-independent. The thermal conductivities of the materials were determined from their thermal diffusivities at room temperature, obtained by means of laser flash experiments. We also determined the variation of the conductivity with the porosity of the cellular glasses. The samples were found to have thermal conductivities in the range 0.08–0.43 W m^{-1} K^{-1}. The dielectric constants of the materials were determined by impedance spectroscopy, and indicated that the materials are insulators. The samples were found to have permittivities in the range 2.6–3.1 S cm^{-1}. These values varied with sample thickness, and appeared to tend towards a limiting value determined by the porosity of the material, or more particularly, by the relationship between the volumes of air and matter in the sample.

Keywords: B. Grain size; B. Porosity; C. Electrical conductivity; C. Mechanical properties; C. Thermal conductivity; D. Glass; Cellular materials

1. Introduction

This paper extends our previous characterisation of cathode-ray tube (CRT) waste glasses, the foam glass elaboration process, and physical and chemical properties of foam glasses [1–4]. Here we report the mechanical, thermal and electrical properties of foam glasses prepared from CRT waste glasses, data that are essential to evaluating the possible applications of these materials [4]. These properties have been studied by Bernardo et al. [5–9]. In their work, the foam glass was elaborated from just panel CRT's glass (lead-free) or with a small quantity of funnel CRT's glass [9].

Firstly, we describe the foam glass elaboration process. Secondly, we present the results of our density and porosity measurements, as well as SEM micrographs from which we determined the microstructures of the expanded materials. The mechanical properties were determined by compressive and flexural measurements. We used our results for these properties to carry out a theoretical modeling study of the cellular glass structures. Lastly, we present the thermal properties, obtained by means of laser flash measurements, and the electrical properties, obtained by impedance spectroscopy.

2. Experimental procedures

2.1. Processing

Various mixtures of a glass powder sample and a reducing agent were prepared. The glass powder samples used were either funnel or panel glass, or a 2:1 mixture (by weight) of panel and funnel glasses. Two reducing agents were used, TiN (Alfa Aesar, ref. 014510, particle size <10 μm) or SiC (Aldrich Chemical, ref. 409-21-2, particle size <63 μm), in amounts of 4 and 5 wt.%, respectively. Granulometry [4] was carried out on the glass powder mixtures (particle size <63 μm) by using a Malvern Instruments Hydro 2000 MU module and the data processing software Mastersizer 2000; the mixtures were then combined with a binder (Arabic gum, 2 mL of 1 wt.% aqueous solution), and prepared by uniaxial

* Corresponding author. Tel.: +33 4 67 143294; fax: +33 4 67 144290.
E-mail address: fmear@lpmc.univ-montp2.fr (F. Méar).

0272-8842/$32.00
doi:10.1016/j.ceramint.2005.11.002

dry-pressing into disc shapes with a diameter of 40 mm and a thickness of 6 mm, using a pressure of 5 tonnes. Expanded products were obtained in pebble form after heat treatment at 750 °C for 120 min under air atmosphere in an electrical furnace. Previous TGA/DTA analyses have shown that the reaction begins near 650 °C [10]. 750 °C was the chosen because it allows to obtain homogeneous foam glass samples with narrow pore size distribution [4,10] and is close to temperature used by Bernardo et al. [7,9]. This temperature is also higher than the T_g of both funnel and panel glasses which are close to 480 and 520 °C, respectively [1,4]. The diameter expansion was found to be on the order of 10–100%, with a thickness expansion on the order of 10–150%.

2.2. Microstructural characterisation

The pore surface and pore morphologies of the foam glasses were investigated by scanning electronic microscopy using a HITACHI S-4500 I. A voltage of 5–10 kV was used in all the observations.

2.3. Density–porosity

The bulk density was measured with helium pycnometry (Micromeritics AccuPyc 1330). The total porosity was obtained from the bulk density and the powder density using the following equation (1):

$$\%\,\text{Porosity} = \left(1 - \frac{\text{bulk density}}{\text{powder density}}\right) \times 100 \quad (1)$$

The open porosity and closed porosity were obtained with helium pycnometry and mercury porosimetry using a Micromeritics Autopore II 9220 instrument. The results varied depending on the initial composition. In all cases, lower porosities were obtained for foam glasses derived from panel glass and higher porosities were obtained for those derived from funnel glass.

2.4. Mechanical testing

2.4.1. Flexural strength

The specimens were machined into 45 mm × 4 mm × 3 mm test bars for bending strength measurements. All the surfaces of the test bars were ground on an 800-grit diamond wheel, and their edges were bevelled. The three-point bending strength was measured for specimen bars with a span of 30 mm at a cross-head speed of 2 mm min^{-1}, using a Dynamat X101 testing machine. Each final result was the average of five measurements.

2.4.2. Compressive testing

Square foam glass samples of 12.5 mm length and 5 mm × 5 mm section area were subjected to uniaxial compressive loading. The tests were conducted at a cross-head speed of 2 mm min^{-1} on the same testing machine as used for the flexural strength measurements. The edges of each traction surface were chamfered using 800-grit SiC paper before testing.

2.5. Thermal and electrical properties

2.5.1. Electrical conductivity measurements

The ac conductivity, $\sigma_{ac}(\omega, T)$, of each sample was measured using a dielectric spectrometer (Novocontrol, BDS 4000) working at a variable frequency f (where $f = 2\pi/\omega$) in the range 10^{-2} Hz to 1 MHz in air and room temperature. The sample was placed in the measuring cell of a dielectric spectrometer [11]. Measurements were performed on disc-shaped samples, which were obtained using a diamond disc saw (Buehler Isomet 2000). The maximum diameter of the samples was 40 mm and their thickness varied from 1 to 10 mm.

2.5.2. Thermal conductivity measurements

The laser flash method was used to determine the thermal conductivities of the samples at room temperature. In this method, a short pulse (0.5 ms) of a laser beam (considered in theory as a Dirac function) is used to heat the front face of a cylindrical sample (10 mm diameter and 2 mm thickness). The absorbed heat diffuses throughout the sample and an infrared detector is used to monitor the evolution of the back face temperature. Samples were coated with a thin graphite layer to improve their laser beam absorption and the emitted thermal signal from the back face.

The thermal conductivity of each sample was calculated from its thermal diffusivity α, heat capacity C_p, and density ρ, using the following standard expression:

$$\lambda = \alpha C_p \rho \quad (2)$$

The specific heat capacity of each foam glass sample was measured using a differential scanning calorimeter (Netzsch DSC 200) for the temperature range from room temperature to about 1200 K.

3. Results and discussion

3.1. Microstructural characterisation

Fig. 1 shows SEM micrographs of foam glasses elaborated from funnel glass with the SiC and TiN reducing agents, respectively. Microstructural characterisation has been more developed in a previous paper, where effects of temperature, reaction time and reducing agent content on the synthesis of macroporous foam were studied [12].

The micrograph of the sample reduced with SiC shows the presence of very fine cells. Mercury porosimetry indicates a single and very narrow pore size distribution, which in fact reflects the size of the ''windows'' between the connected cells [13] (the black stain on the cell surface); this single distribution of pores was determined by SEM. We observed a fully interconnected uniform structure with cells connected to all their neighbours.

The micrograph of the sample reduced with TiN reveals it has a double distribution of cells. It appears that the material have both ''cell windows'' and ''pores'': the voids in the cell walls. Mercury porosimetry was used to characterise this double distribution of cells sizes. In this sample, the smaller

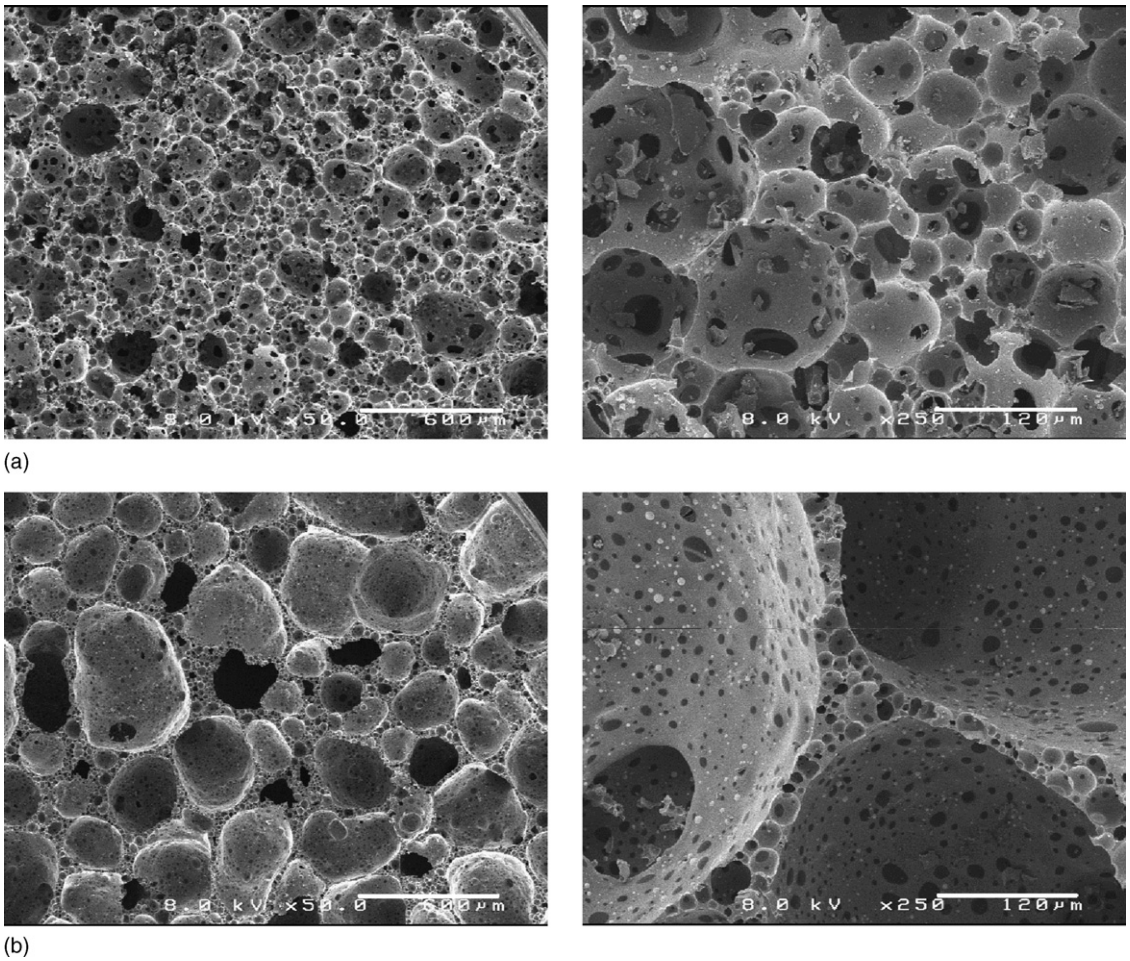

Fig. 1. Foam glass sample elaborated from funnel glass with (a) SiC (750 °C for 120 min) and (b) TiN (750 °C for 120 min).

cells are distributed throughout the regions between the larger cells. This distribution could induce coalescence phenomena or coarsening phenomena, when smaller pores are likely to be dissolved in larger pores which are favoured by a decrease of the surface energy of the system [7]. This microstructure is similar to that of other foams, including those not elaborated from glasses, such as metallic foams, polymer foams and ceramic foams [14,15]. In these materials, the heterogeneous of the cell size is conserved. On the other hand, the metallic foam microstructure can be controlled and the foams feature cells of relatively uniform size [16].

3.2. Mechanical testing

An example of the shape curve obtained during compression testing is shown in Fig. 2. This curve indicates the variation of the deformation of material with the applied stress. This shape is very similar to those obtained by Tasserie [17] in case of expanded materials. In our cases, we only observed the initial stages of compression. The plateau and subsequent increase in density suggested by Gibson and Ashby [18], have not been observed.

Three zones can be distinguished:

- Zone I: for low compressions, the material is deformed elastically.
- Zone II: the discontinuity in the curve in zone II indicates the rupture of the weakest individual elements of the material, in this case the celled wall face of the material. The fracture of an element leads to the redistribution of the compression (of stronger intensity) in its vicinity. At the end of zone II, the material has incurred more or less marked damage.
- Zone III: this local damage leads to total fracture.

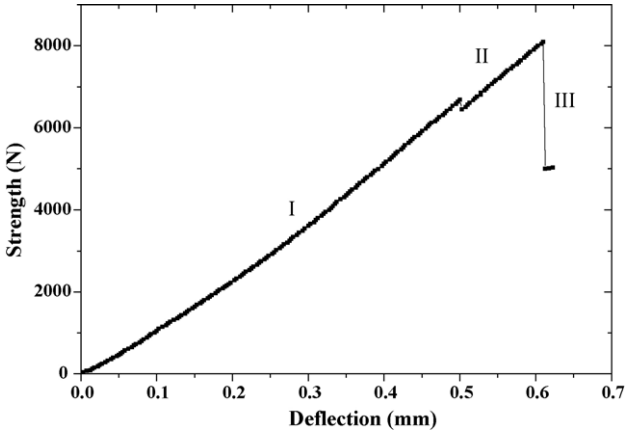

Fig. 2. Shape of the curve obtained from a compression test.

Table 1
Results of the failure stress under compression tests for samples of various compositions

Compressive test	SiC (5 wt.%)			TiN (4 wt.%)		
	Panel	Funnel	Mixed	Panel	Funnel	Mixed
Porosity (%)	3.7 (0.1)	84.5 (1.7)	46.5 (0.9)	50.1 (1.0)	86.1 (1.7)	67.9 (1.4)
σ (MPa)	267 (17)	4	60	99 (11)	4	24
K (GPa)	5.4 (0.1)	0.5 (0.2)	4.4 (1.0)	4.7 (0.8)	0.4 (0.1)	1.9 (0.2)

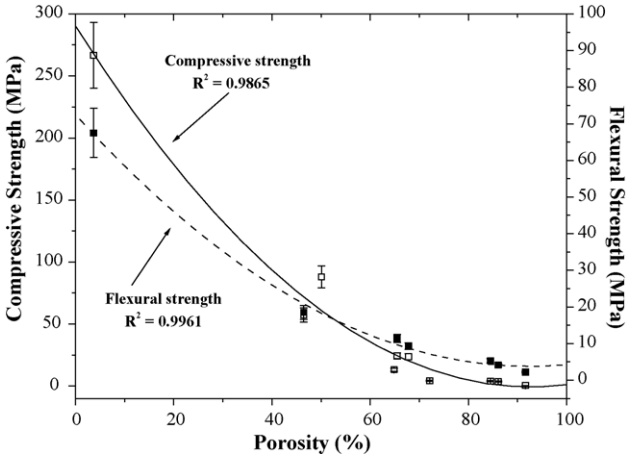

Fig. 3. Compressive strength and flexural strength vs. porosity for various samples.

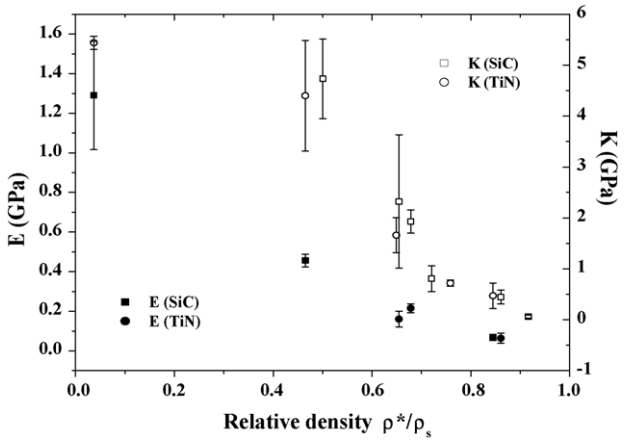

Fig. 4. Variation with porosity of the Young modulus E and the bulk modulus K.

The results for the failure stress obtained from the compression tests are shown in Table 1. Weibull statistic is used to provide compressive strength values [10,17]. This statistic study requires at least twenty mechanical tests. In the case of panel CRT's glass (porosity is higher), on the other hand, we have only used the average of 10 tests.

It has been observed that the reaction process (following the reaction: $PbO + SiC \rightarrow Pb + SiO_2 + CO_2$) is limited to panel glass because the reaction involves lead oxide [4,10]. The lead oxide content in the initial panel glass is higher and therefore so is the resulting metallic lead content, this has the effect of making the cell size diameter larger. The compressive strength is shown as a function of the volume fraction of porosity in Fig. 3a). As the porosity increases, the compressive strength decreases; the lowest value recorded was 4 MPa. Exponential function was found to provide the best fit to the decrease in compressive strength with increase in porosity.

The results of the flexural strength measurements are shown in Table 2. The values were found to vary with the volume fraction of porosity. The flexural strength was found to be lowest for the highest porosity; the lowest value recorded was 4 MPa. The flexural strength is shown as a function of the volume fraction of porosity in Fig. 3b).

As used in the case of compressive strength, an exponential function provides the best fit. The failure trends follow the exponential equation proposed first by Ryshekewitch and Duckworth [19,20] (Eq. (3)):

$$\sigma_f = \sigma_0 e^{-bP} \tag{3}$$

where σ_f is the strength of the porous structure with respect to compression, σ_0 the strength of the non-porous structure, P the volume fraction of porosity, and b is an empirical constant [19,20].

In Fig. 4, we show the variations with porosity of the Young modulus E and the bulk modulus K for the foams obtained with the TiN and SiC reducing agents. K and E were computed from stress/strain curves, without taking into account the rigidity of the equipment itself in regard to the relatively low values obtained. There is no significant difference between the results

Table 2
Results for the flexural strengths of samples of various compositions

Flexural strength	SiC (5 wt.%)			TiN (4 wt.%)		
	Panel	Funnel	Mixed	Panel	Funnel	Mixed
Porosity (%)	3.7 (0.1)	84.5 (1.7)	46.5 (0.9)	50.1 (1.0)	86.1 (1.7)	67.9 (1.4)
σ (MPa)	68 (12)	5 (0.9)	19 (1)	21 (1)	4 (1)	9 (1)
E (GPa)	1.30 (0.20)	0.07 (0.01)	0.45 (0.03)	0.41 (0.02)	0.07 (0.02)	0.22 (0.02)

for the two reducing agents; the differences lie within the experimental error. From E and K we can determine the Poisson ratio ν:

$$\nu = \frac{1}{2} - \frac{E}{6K} \tag{4}$$

The Poisson ratio ν determined from this equation was found to be porosity-independent, approximately 0.475 ± 0.015. This value is very close to 0.5, which is the value for incompressible materials such as liquids, and is different from that predicted by Gibson and Ashby ($\nu = 0.33$) [18]. However, it is well known that it is difficult to determine ν precisely, notably in the case of static indirect measurements [18]. Thus, it must be kept in mind that ν only appears to be porosity-independent.

Some previous experimental and theoretical studies have concluded that ν is porosity-independent [18,21,22], whereas other studies [23–25] have reached different conclusions. However, following Rice [21] we believe that observations of variation with porosity of ν could be due to inhomogeneities of the porosity in their samples. Therefore, in our study, we analyse the porosity dependences of the other elastic properties of our glass foams by excluding theoretical models that use porosity-dependent Poisson ratio ν [23–25]. From ν we can determine the shear modulus G:

$$G = \frac{E}{2(1+\nu)} \tag{5}$$

Because ν is porosity-independent and close to 1/2, $G \cong E/3$, and has exactly the same porosity-dependence as E. Thus, only the porosity dependence of E need be analysed.

From a general point of view, the physical and in particular the mechanical properties of porous materials and foams are dependent on the type of porosity and the amount of pores (porosity P). Previous studies of porous materials and foams have not examined the effect of cell size on the mechanical properties of these materials, likely because pore size is expected to have an insignificant effect on these properties.

The mechanical properties of foams and porous materials have been widely studied. Many authors have studied the variation of mechanical properties with porosity using simple phenomenological models in which the parameters do not have any physical meaning, for example, f (Eq. (6)), [25,26] or using models taking into account only one type of porosity [21,25–29], which is obviously not very realistic. Some authors, however, have tried to build models in which the parameters include information about the type of porosity (open or closed) [18], the shapes of the pores (cylindrical or spherical) [21–24,30] and the growth mechanisms of these materials [31].

These models predict different types of porosity-dependence. The first model we discuss makes use of scaling laws. For the general case of the percolation model [26]:

$$E = E_0 \left(\frac{P_c - P}{P_c} \right)^f \tag{6}$$

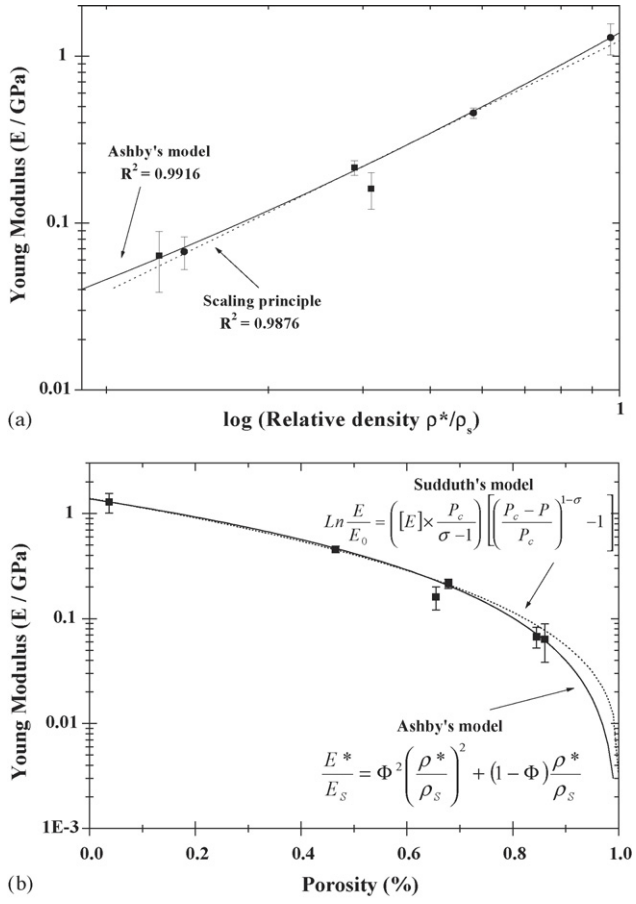

Fig. 5. Comparison of the experimental variation with porosity of the Young modulus E with the predictions of the models of (a) Scaling and Ashby and (b) Sudduth and Ashby.

where P_c is the critical porosity at which $E = 0$ (which can be different to 1), and E_0 is the Young modulus of the bulk material ($P = 0$). For the materials we are discussing, $E_0 = 1$. If a double-logarithmic plot of E versus $1 - P$ (Fig. 5b)) is drawn, we find $f = 1.57$. This value is slightly larger than that found for porous ThO_2 by Kovacik ($f = 1.20 \pm 0.07$) [31], but smaller than the value of $f = 2.1$, which is the theoretical prediction when the dimensions of the system go to infinity [31].

Other authors [23,29] have also developed similar models for the variation of properties with porosity. However, the model of Arnold et al. [23] requires that the majority of the pores must be spherical and that the porosity must be essentially closed (even in the case of high porosity), which is not in accord with our experimental data. Moreover, this model predicts that the Poisson ratio is not independent of P [23].

Wagh's model [29] for the case of cylindrical pores predicts that, in this case, n (empirical parameter without physical signification such as f) should be greater than or equal to 2, in agreement with Ashby's model [18,29]. Thus, for our samples, both spherical and cylindrical pores should be present (if we consider only the case of ideal pores), with both closed and open porosity in our foams, as observed experimentally.

Ashby's model [18] is better than other models because it can be used to determine the ratio ϕ between the open and the

total porosity by making the approximation that this ratio remains constant in the complete porosity range (which is not obviously the case in reality). In this model, we have:

$$\frac{E^*}{E_s} = \Phi^2 \left(\frac{\rho^*}{\rho_s}\right)^2 + (1-\Phi)\frac{\rho^*}{\rho_s} \quad (7)$$

where ρ_s is the bulk density (for $P = 0$), ρ^* the density of the foam, and ϕ is the volume fraction of the solid contained at the cell edges; the remaining fraction $(1 - \phi)$ is on the faces [18]. If the foam is open-celled, the pores are fully interconnected, with no material in the hypothetical walls, so that $\phi = 1$, on the contrary, for a closed-cell foam, $\phi = 0$ [7]. P is the porosity content, therefore: $1 - P = \rho^*/\rho_s$.

In Fig. 5a, we show on a double-logarithmic scale a fit of the experimental data with Eq. (7) using $\phi = 0.82$ and $E_0 = 1.62$ GPa (experimental values).

Among the other models found in the literature, only Sudduth's model [26] provides a good fit of the experimental data. In this model, we have:

$$\ln \frac{E}{E_0} = \left([E] \times \frac{P_c}{\sigma - 1}\right)\left[\left(\frac{P_c - P}{P_c}\right)^{1-\sigma} - 1\right] \quad (8)$$

where P_c is the critical porosity with $E = 0$ and $P_c = 1$, E_0 the bulk Young's modulus ($E_0 = 1.4$ GPa), σ the particle interaction coefficient and also a fitting parameter ($\sigma = 0.67$), and $[E]$ is the intrinsic modulus (we use this parameter only as a fitting parameter ($[E] = -2.1$)); these two parameters provide some information about the growth mechanisms of the foam glasses. The value of σ found here is very close to that found in the case where the particle compaction that occurs at the start of the appearance of the pores occurs in an undistorted manner. However, the value of $[E]$ lies between the value obtained in this case and that obtained for the misalignment of the particles (and therefore of the pores) with a shearing component. In fact, $[E]$ is closer to that obtained for this latter case. Thus, we propose that either there is no distortion during the formation of the pores, or there is a weak distortion with a shear component.

These results seem to be in good agreement with the SEM microstructures, in which we see no or only weak distortion of the spherical and cylindrical pores present in our samples.

The results of fitting the data with Eq. (8) are given in Fig. 5b) for a semi-logarithmic scale, along with the fit using Eq. (7). Finally, we unsuccessfully tried to fit the experimental variation of E with porosity with combinations of the formula suggested by Rice [30], $E = E_1 + E_2$, where $E_1 \propto e^{-bP}$ and $E_2 \propto 1 - e^{-b'(1-P)}$ implement the minimum solid area model of Rice [30] at low and high porosities, respectively.

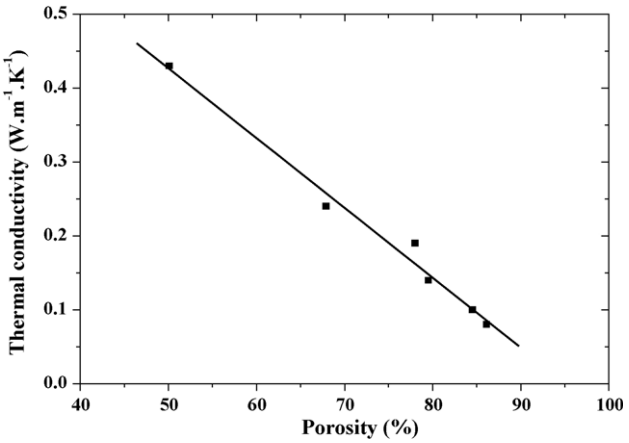

Fig. 6. Thermal conductivity vs. porosity for various samples.

Indeed, Rice [30] has shown that many materials follow this law for low porosities (typically $P < 0.5$). If we assume that this is true for our materials, we find $b = 2.5$ for $P < 0.5$; in this porosity range, the proportion of closed pores (and therefore of spherical pores) will be higher than for the previously studied case of $P > 0.5$. This value for b lies between that for cubic (or random) stacking of spherical pores ($b = 3$) and that for cylindrical pores ($b = 1.4$) [30].

3.3. Thermal and electrical properties

3.3.1. Thermal properties

The results for the thermal conductivity are shown in Table 3. The thermal conductivity was found to vary from 0.08 (funnel CRT's glass and 4 wt.% TiN) to 0.43 (panel CRT's glass and 4 wt.% TiN) with increasing porosity.

The variation of the thermal conductivity with porosity is shown in Fig. 6. The thermal conductivity increases with decreasing porosity. As can be seen, this decrease is linear; this variation is different to that of the mechanical properties with porosity, in that the variations of the compressive and flexural strengths with porosity were exponential. The thermal

Table 3
Thermal conductivities obtained from laser flash experiments

Sample			Density (kg m^{-3})	Porosity (%)	Specific heat (J kg^{-1} K^{-1})	Thermal diffusivity (m^2 s^{-1})	Thermal conductivity (W m^{-1} K^{-1})
Composition	T (°C)	t (min)					
Mixed-SiC	850	60	375	79.5	800	4.74×10^{-7}	0.14
Mixed-TiN	850	60	499	78.0	800	4.74×10^{-7}	0.19
Funnel-SiC	750	120	460	84.5	800	4.73×10^{-7}	0.10
Funnel-TiN	750	120	378	86.1	800	4.73×10^{-7}	0.08
Mixed-TiN	750	120	878	67.9	800	4.75×10^{-7}	0.24
Panel-TiN	750	120	1350	50.1	800	4.78×10^{-7}	0.43

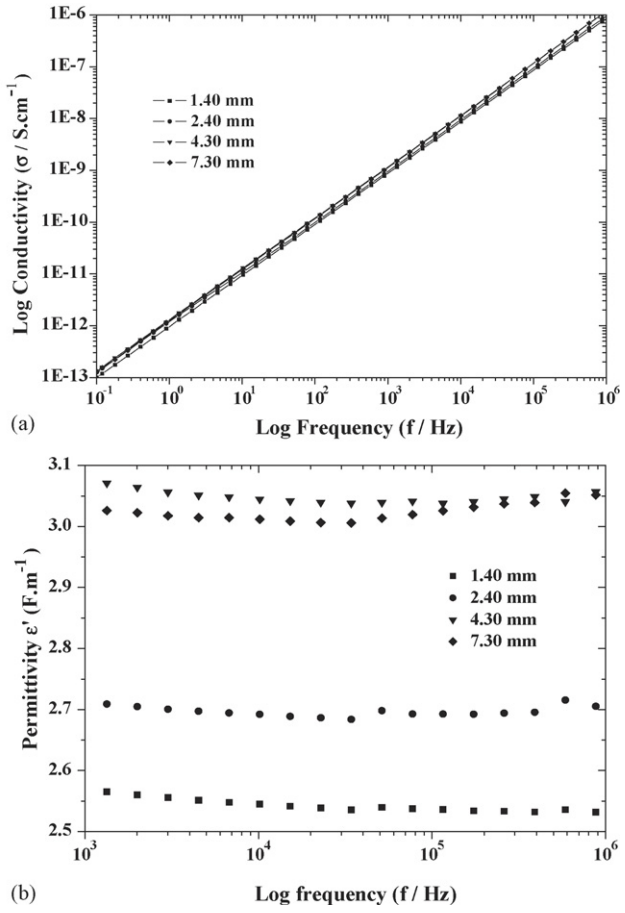

Fig. 7. (a) Logarithmic conductivity vs. logarithmic frequency for various sample thicknesses. (b) Permittivity vs. logarithmic frequency for various sample thicknesses.

conductivity of air at room temperature is 0.023 W m^{-1} K^{-1}. As the porosity increases, the thermal conductivity tends towards the thermal conductivity of air; its largest value is equal to bulk glass values (0.75–1.45 W m^{-1} K^{-1}).

Samples with conductivity lower than 0.25 W m^{-1} K^{-1} are classified as insulating materials, which was found to be the case for all the samples analyzed except those containing panel glasses, which have low porosity and strong thermal conductivity (0.43 W m^{-1} K^{-1}).

3.3.2. Electrical properties

The variations of the dielectric conductivity of the samples with frequency obtained with impedance spectroscopy are shown in Fig. 7a) for various sample thicknesses; these variations are not dependent on the reducing agent, so only results for samples elaborated with funnel CRT's glass and 5 wt.% SiC are shown.

Note that the thickness does not have any influence on the conductivity, and that the logarithm of conductivity increases linearly with log f. This result is explained by the absence of diffusive phenomena, as shown by Fig. 8. In this case: $\sigma'(\omega) = \sigma'_{pol}(\omega)$.

The variations of the "apparent real permittivity" ε' with the logarithm of the frequency are shown in Fig. 7b). For the same samples (same compositions), the real permittivity varies from 2.5 to 3.1 F m^{-1} with increasing thickness of the material. It increases for initial increases in the thickness of the sample, then for greater thickness does not appear to increase any further. The permittivity thus seems to tend towards a limiting value determined by the porosity of the material, or more particularly, by the relationship between the amounts of air and matrix in the sample (Fig. 8).

As the sample thickness increases, the capacity C, in the case of "linear-isotropic-homogenous" samples, models by a stack capacities with alternating matter (vitreous matrix) and air (pore). With this model the variation of the permittivity with thickness can be explained, which in the case of "linear-isotropic-homogenous" materials should theoretically not increase.

Using the model developed by Maxwell–Eucken, thermal conductivity of the materials is also calculated using the simple rule of mixture [32]. Using this model, the permittivity of the material could be determined precisely.

Unlike the mechanical and thermal properties, the pore diameter has only a negligible effect on the electric conductivity

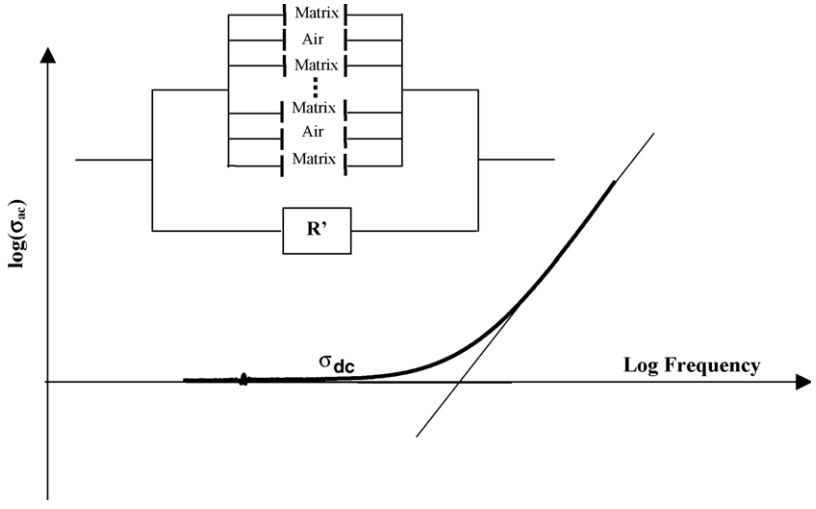

Fig. 8. Theoretical logarithmic conductivity vs. logarithmic pulsation for the conductivity σ_{dc} determination and schematic electrical modeling.

Table 4
Relative permittivities of various reference materials

References and materials	Relative permittivity (25 °C)
Foam glass elaborated from CRT	2.1–3.1
Air	1
Foamglas [34]	5–7.2
Polyurethane foam	1.7
Thin layer of porous silice [35]	1.70
Panel glass	10.2
Glass $CaO–B_2O_3–SiO_2$ [36]	4.97

(and permittivity) of the foam glasses [33]. Table 4 presents the relative permittivity values of some materials for comparison.

4. Conclusions

In this study, we determined the specific properties of foam glasses obtained from waste CRT glasses. The fragile character of glasses remains in this material. In spite of its high porosity, these materials exhibited high rupture stresses: 4–267 MPa for the compressive strength and 4–68 MPa for the flexural strength.

Our modelling of the cellular structure showed, by taking into account the porosity-independence of the Poisson ratio, that the model suggested by Gibson and Ashby [18] is the most appropriate for these materials.

Our results regarding the thermal properties of the foam glasses indicated that the thermal conductivity is strongly affected by the porosity. Specifically, the conductivity was found to decrease linearly with the porosity. These results (values lower than $0.25\ W\ m^{-1}\ K^{-1}$) indicate that these materials, except the panel glass elaborated samples, are heat insulators.

Lastly, our investigation of the dielectric properties of these materials showed that their conductivity (σ_{dc}) (referring to the diffusive phenomena of the charge carriers) is lower than that of window glass ($=1.0 \times 10^{-13}\ S\ cm^{-1}$).

The absence of the σ_{dc} plateau, as we can see in Fig. 8 in this interval of frequency, characterized absence of charge carriers in our samples.

Acknowledgments

The work presented in this paper was carried out by a Technological Team of Research, ERT 3 ‘‘Caractérisation des Matériaux’’, created by the French ‘‘Ministère de la Recherche et de la Technologie’’ (MRT). The authors thank the MRT and ANRT (Association Nationale de la Recherche Technique) for their financial support. IBM Corporation and APF Industrie agencies of Montpellier (France) are gratefully acknowledged, as well as Mr. B. Meyrand and C. Rey for their collaboration.

References

[1] F. Mear, P. Yot, M. Cambon, B. Liautard, Verre Rev. 9 (1) (2003) 33–41.
[2] F. Mear, P. Yot, M. Cambon, B. Liautard, Verre Rev. 9 (2) (2003) 72–77.
[3] F. Mear, P. Yot, M. Cambon, M. Ribes, Waste management, (2006) in press.
[4] F. Mear, PhD thesis, Montpellier University, France, 2004.
[5] E. Bernardo, G. Scarinci, S. Hreglich, J. Eur. Ceram. Soc. 23 (2003) 1819–1827.
[6] E. Bernardo, R. Castellan, S. Hreglich, Ceram. Int., in press.
[7] E. Bernardo, F. Albertini, Ceram. Int., in press.
[8] E. Bernardo, G. Scarinci, A. Maddalena, S. Hreglich, Compos.: Part A 35 (2004) 17–22.
[9] E. Bernardo, G. Scarinci, S. Hreglich, Glass Sci. Technol. (Glastechnische Berichte) 78 (2005) 7–11.
[10] F. Mear, P. Yot, M. Cambon, M. Ribes, Adv. Appl. Ceram. 104 (3) (2005) 123–130.
[11] http://www.novocontrol.de/html/index_sample_cells.htm.
[12] F. Mear, P. Yot, M. Ribes, Mater. Lett. 60 (2006) 929–934.
[13] A. Desforges, M. Arpontet, H. Deleuze, O. Mondain-Monval, React. Funct. Polym. 53 (2002) 183–192.
[14] H. Deleuze, B. Maillard, O. Mondain-Monval, Bioorg. Med. Chem. Lett. 12 (2002) 1877–1880.
[15] A. Mercier, H. Deleuze, O. Mondain-Monval, React. Funct. Polym. 46 (2000) 67–79.
[16] C. San Marchi, A. Mortensen, Acta Mater. 49 (2001) 3959–3969.
[17] M. Tasserie, Ph.D. thesis, Rennes University, France, 1991.
[18] L.J. Gibson, M.F. Ashby, Cellular solids: Structure and properties, second ed., Cambridge Solid state Press, Cambridge University Press, 1997.
[19] R. Ryshkewitch, J. Am. Ceram. Soc. 36 (1953) 55.
[20] W. Duckworth, J. Am. Ceram. Soc. 36 (1953) 68.
[21] R.W. Rice, J. Mater. Sci. 31 (1996) 1509–1528.
[22] O. Yeheskel, O. Tevet, J. Test. Evaluat. 28 (2000) 189.
[23] M. Arnold, A.R. Boccaccini, G. Ondracek, J. Mater. Sci. 31 (1996) 1643.
[24] L.-P. Chao, J.H. Huang, Y.-S. Huang, J. Compos. Mater. 33 (1999) 2002.
[25] N. Ramakrishnan, V.S. Arunachalam, J. Mater.Sci. 25 (1990) 3930.
[26] J. Kovacik, J. Mater. Sci. Lett. 20 (2001) 1953–1955.
[27] T.E. Matikas, P. Karpur, S. Shamasundar, J. Mater. Sci. 32 (1997) 1103–1109.
[28] K.K. Phani, J. Mater. Sci. 31 (1996) 262.
[29] A.S. Wagh, R.B. Poeppel, J.P. Singh, J. Mater. Sci. 26 (1991) 3862.
[30] R.W. Rice, J. Mater. Sci. 31 (1996) 102–118.
[31] R.D. Sudduth, J. Mater. Sci. 30 (1995) 4451–4462.
[32] N.P. Bansal, D. Zhu, Ceram. Int. 31 (2005) 911–916.
[33] Y. Feng, H. Zheng, Z. Zhu, F. Zu, Mater. Chem. Phys. 78 (2002) 196–201.
[34] Foamglas Specification Sheet, Pittsburgh Corning, February 2000.
[35] J.-Y. Zhang, I.W. Boyd, Mater. Sci. Semiconductor Process. 3 (2000) 345–349.
[36] S.-H. Wang, H.-P. Zhou, Mater. Sci. Eng. B99 (2003) 597–600.